

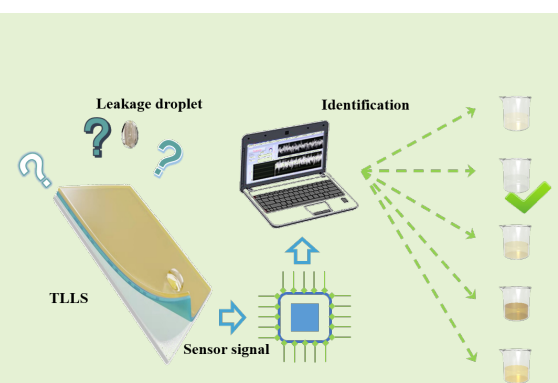
A Liquid-solid Triboelectric Sensor for Minor and Invisible Leakage Monitoring in Ship Pipelines

(May 2023)

Xinyu Wang, Xiaodong Jiao, Pengyu Liang, Zelin Fei, Wenxuan Guo, Jinshan Yang, Tangzhen Guan, Hao Sun, Jin Tao, Xianyi Zeng, *IEEE Senior Member, IEEE*, Xuyuan Tao, Xingjia Jiang, Peng Xu, Minyi Xu and Qinglin Sun

Abstract— Ship pipelines are the most efficient and cost-effective devices for liquid transportation. However, pipeline leakage can pose a threat to ship operation, human safety, and marine environment, especially for minor or invisible leakage with insufficient monitoring. Herein, we propose a triboelectric liquid leakage sensor (TLLS) based on a liquid-solid triboelectric nanogenerator (TENG), aiming at detecting, locating, and identifying the invisible and minor leakage of the ship pipelines in real time. The proposed device mainly consists of a steel electrode and SiO₂/PTFE coating. When the coating contacts and separates from the leakage droplets, it generates electric signals that reflect the information of the droplets, such as their angle, temperature, height, volume, and type. The coating also has self-cleaning, superhydrophobic and wear-resistant properties, making it suitable for environments with vibration, high temperature, and humidity. In addition, the coating exhibits the potential to integrate with the prevailing ship steel structures, thereby enabling the formation of extensive sensor arrays for detecting leakages. From the experimental data analysis, the TLLS can obtain accurate information of minor or invisible leakage droplets. Moreover, an intelligence identification system based on the TLLS arrays and a lightweight artificial neural network is successfully developed. To highlight the stability and scalability of the developed system, real-time liquid droplet detection and identification are performed, showing great potential for ship pipeline monitoring and provides an intelligent method for modern ship management.

Index Terms— Liquid-solid triboelectric sensor, Self-powered, Ship pipeline monitoring, Invisible and minor liquid leakage.



This work was supported by the National Natural Science Foundation of China(Grant No.61973172, 62003177, 62103204, 62003175 and 61973175), Joint Fund of the Ministry of Education for Equipment Pre research(Grant No.8091B022133) and General Terminal IC Interdisciplinary Science Center of Nankai University. (Corresponding authors: Peng Xu, Minyi Xu, and Qinglin Sun.)

Xinyu Wang, Xiaodong Jiao, Pengyu Liang, Wenxuan Guo, Jinshan Yang, Hao Sun, Qinglin Sun are with College of Artificial Intelligence, Nankai University, Tianjin, 300350, China (e-mail: sunql@nankai.edu.cn).

Zelin Fei is with Tsinghua University, Beijing, 100084, China.

Xianyi Zeng and Xuyuan Tao are with ENSAIT, University of Lille, 2 allé e Louise et Victor Champier, 59056 Roubaix Cedex 1, France.

I. INTRODUCTION

THE ship pipelines are the significant components of the ship in the use of liquids transportation [1], ensuring the stability of the voyage and meet the needs of the crew and passengers [2]. However, pipeline leakage can pose a

Jin Tao is with Silo AI, Helsinki 00100, Finland.

Tangzhen Guan, Peng Xu, Xingjia Jiang, and Minyi Xu are with Dalian Key Laboratory of Marine Micro/Nano Energy and Self-powered Systems, Marine Engineering College, Dalian, Maritime University, Dalian, 116026, China (e-mail: xuminyi@dlu.edu.cn).

threat to ship operation, human safety, and marine environment [3]. It can be typically caused by vibration, high temperature, corrosion, or sabotage [4], [5]. Manual inspection is the most common method for detecting pipeline leakage. It has high accuracy for larger leakage locations but is limited by the responsibility and experience of the inspector. Several leakage detection technologies have been developed based on different types of sensors [6], such as acoustic [7], infrared [8], fiber optic [9], and ultrasonic flow sensors [10]. These sensors rely on pressure, temperature, density, flow rate or sonic velocity to detect and locate pipeline leakage. However, they have low sensitivity to minor or invisible leakage that can affect the performance and safety of pipelines [11], [12]. For example, traditional ultrasonic pipeline inspection has limitations [13] in application due to wave propagation attenuation, especially in complex fluids and high-pressure pipelines [14]. Furthermore, Fiber optic sensors face challenges related to complex installation, costly and intricate replacement, and vulnerability to noise [15] and variations in light transmission, posing difficulties in detecting subtle or concealed leaks [16]. Therefore, designing an effective sensor for detecting minor or invisible leakage in ship pipelines is still a challenge.

Triboelectric nanogenerator (TENG) based on the coupling principle of triboelectrification effect and electrostatic induction has many impressive applications in low-frequency energy harvesting [17]–[19] and self-powered sensing [20]. It attracts worldwide attention due to its advantages of high output performance, high sensitivity, diverse material options, and low cost [21]–[23]. Various triboelectric sensors have been developed for wave sensing [23]–[25], vortex sensing [26], [27], speed sensing [28], [29], tactile sensing [21], [30], and wind sensing [31], [32]. These sensors can sense the object or condition factors autonomously without external electric or optical signals. However, there is still a lack of effective sensors for detecting minor or invisible leakage in ship pipelines, which can pose a threat to ship operation, human safety, and marine environment [1], [33]–[35]. Motivated by the aforementioned, we propose a novel triboelectric self-powered sensor that can detect, locate, and identify minor or invisible leakage in ship pipelines.

Most studies on triboelectrification and electrostatic induction have focused on the solid-solid interface [36]. However, this type of triboelectric sensor is not suitable for high-humidity environments, such as ship pipelines transporting

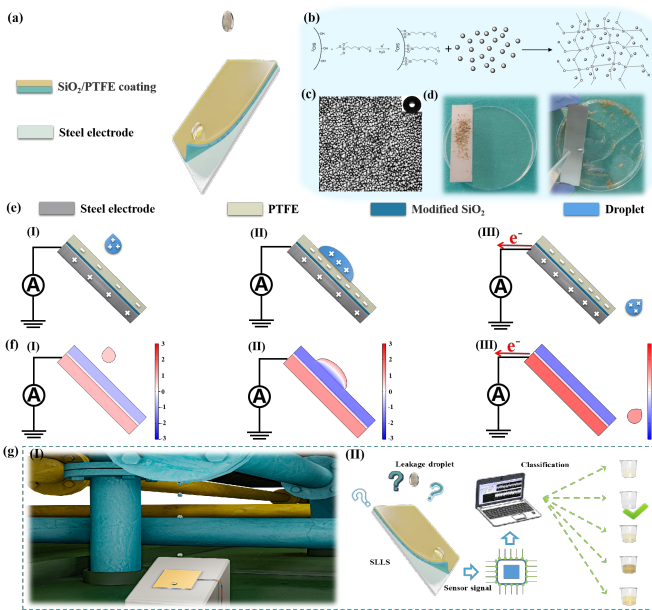
multiphase fluids, because moisture can reduce the triboelectric charge and impair the sensor performance [37]–[39]. In contrast, liquid-solid triboelectric sensors have advantages in moist environments, as they are less affected by environmental humidity [40]. Conventional liquid-solid triboelectric sensors have drawbacks of complex fabrication methods, low dimensional control, and high cost. To overcome these challenges, we propose using superhydrophobic interfaces to enhance the contact and separation between liquid and solid phases. This can improve the stability, accuracy, and efficiency of the liquid-solid triboelectric sensor [41]. Therefore, designing a superhydrophobic triboelectric coating material is a key step for developing a liquid-solid triboelectric sensor for ship pipeline leakage detection.

In this paper, a triboelectric liquid leakage sensor (TLLS) based on TENG is designed to capture leakage information and assist in leakage location via liquid-solid contact electrification and electrostatic induction. The sensor consists of a steel electrode and a SiO₂/PTFE superhydrophobic coating that has advantages of superhydrophobicity, self-cleaning, wear-resistance, and easy integration with existing steel structures. On the basis of the above characteristics, the coating can also combine with the existing steel structures of the ships to form large-scale sensor arrays without disassembly. Since there is an electronegativity difference between the leakage droplets and the coating, an electrical signal generates during the dropping and contacting process that contains information about the incident angle, temperature, height, volume, and type of the droplets. From experimental data research and analysis, an induction law is established and an intelligence identification system based on the TLLS arrays and a lightweight artificial neural network is successfully developed. The classification accuracies of the five trial liquids are over 99% due to the steady output performance of the TLLS and the robustness of the intelligence system. To highlight the stability and scalability of the developed system, real-time liquid droplet detection are performed, showing great potential for ship pipeline monitoring and provides an intelligent method for modern ship management.

II. RESULTS AND DISCUSSION

A. Basic structure and working mechanism of the TLLS

The detailed structure of the TLLS is shown in Fig. 1(a), which consists of a steel electrode and SiO₂/PTFE



(a) Schematic structure of the TLLS. (b) Chemical reaction between the SiO₂ and PTFE components. (c) SEM image of the TLLS obtained by field-emission scanning electron microscopy and contact angle obtained by a contact angle analyzer. (d) Schematic diagram of the self-cleaning property. (e) Working principle of TLLS. (f) Potential voltage distribution simulation obtained through COMSOL. (g) Potential applications of the TLLS.

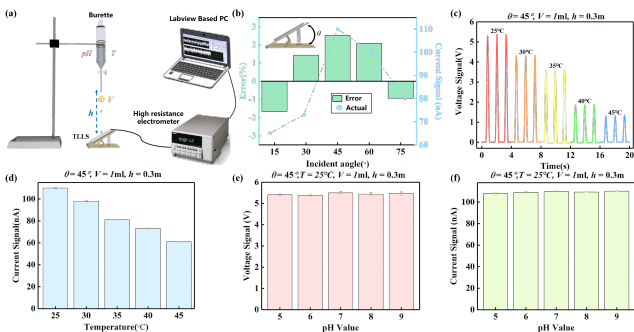
superhydrophobic coating. Micron scaled PTFE particles are hybridized with nano scaled SiO₂ and heat-treated to create a dual surface structure with nano/micron microscopic rough structure with low surface energy. The corresponding chemical equation is shown in Fig. 1(b). According to the SEM of TLLS image obtained by field-emission scanning electron microscopy, the nano/micron microscopic surface structure is shown in Fig. 1(c). With the help of SiO₂/PTFE components, the surface structure of the sensor offers low surface energy and raises the surface roughness, which allows air, water droplets and the interface to form a unique three-phase structure, reducing the contact area between water droplets and the coating when an air film is formed on the surface, thus forming a superhydrophobic phenomenon [42]. A contact angle analyzer is used to investigate the surface characteristics of the TLLS as shown in Fig. 1(c) inset picture. The contact angle of water droplets on the sensor surface reaches 152° demonstrating superhydrophobic properties. It is worth noting that the surface of the normal PTFE tape with a steel electrode is also tested and the water contact angle is only 92°, as shown in Fig. S4. Due to the harsh cabin environment and corrosive

fluids in the pipeline, better hydrophobic capabilities are beneficial to the sensitivity and the service life of the sensor. Fig. 1(d) shows the TLLS's self-cleaning effect associated with the superhydrophobic surfaces, providing high levels of immunity against dust contamination for continuous monitoring.

The mechanical abrasion resistance of the prepared TLLS sample is investigated against 1000 grit SiC sandpaper for 1 m at the applied pressure of 14.4 kPa, which is demonstrated in Fig. S5. The sample is placed face-down to sandpaper and moves for 0.25 m along one direction, then the sample is rotated by 90° (face to the sandpaper) and then moved for 0.25 m along one direction. This process is defined as an abrasion cycle, and repeat the cycle nine times to complete the abrasion test. After the abrasion test, the contact angle of water droplets on the sample surface only decrease from 152° to 151°, effectively maintaining the mechanical integrity of the coating, which is shown in Fig. S6. Fig. 1(e) demonstrates the working principle of the TLLS. The TLLS is installed beneath the leak-prone part of the ship pipeline, since the electrostatic induction effect, opposite electric charges with equal numbers distribute on the surface of the steel electrode and the coating. The leakage droplets lose electrons and become positively charged due to the friction with air during the dropping process. As the droplets make contact with the coating, owing to the electrostatic induction effect, the negative charges on the surface of the coating increase. Then, the superhydrophobic property of the coating allows the leakage to slip off quickly after the contacts. Meanwhile, the positive charge on the steel electrode surface is not enough to screen the negative charge on the friction layer, leading to the generation of current between the electrodes and the ground via electrostatic induction. At this point, the generation of a complete electric power cycle is completed. In addition, the electric potential between the coating and the steel electrode is simulated by COMSOL, as shown in Fig. 1(f), which further validates the working principle of TLLS. Fig. 1(g) shows the potential applications of the TLLS arrays based sensing system in the intelligent ship pipelines, demonstrating a promising way for online liquid leakage information detection, location, as well as classification and evaluation of the liquid type and state.

B. Mechanical and electrical property characterization of TLLS

The complete experimental setup is illustrated in Fig. S7. It includes a supply pump (BTC-600CA) used to drive



(a) The schematic diagram of the experimental setup for measuring performance under various parameters. (b) The output current performance and corresponding errors of TLLS under different incident angle from 15° to 75° . (c) The output voltage performance of TLLS under temperature from 25°C to 45°C . (d) The output current performance of TLLS under temperature from 25°C to 45°C . (e) The voltage response due to different pH value from 5 to 9. (f) The current response due to different pH value from 5 to 9.

the flow of liquid droplets, along with a dropper to simulate minor leakage of liquid droplets ($1-5\text{ml}$) from the pipeline. The vertical distance between the dropper and the triboelectric liquid leakage sensor (TLLS) can be adjusted ($0.1-0.5\text{m}$) to simulate leakage from varying heights. Liquid temperature and pH values are controlled by mixing in a beaker. The setup also comprises the TLLS and an adjustable platform to vary the angle of the TLLS $15-75^\circ$. The electric signals generated when leakage droplets make contact and separate from the TLLS are captured using a Keithley 6517 electrostatic meter. The data is transmitted to a host computer through the NI USB-6363 data acquisition card with a 500 Hz data acquisition rate. Real-time data recording and acquisition are facilitated by the LABVIEW visualization software on the host computer. The primary objective is to characterize leakage droplet parameters, which include incident angle, temperature, pH value, height, volume, and droplet types, as shown in Fig. 2(a). These parameters are defined as Θ , T , pH , h , V , and K , respectively. For each parameter tested, a controlled variable approach is employed to keep other parameters constant, ensuring accurate assessment of the parameter's impact on TLLS response characteristics. It's worth noting that each parameter measurement is repeated over 10 times to obtain average values.

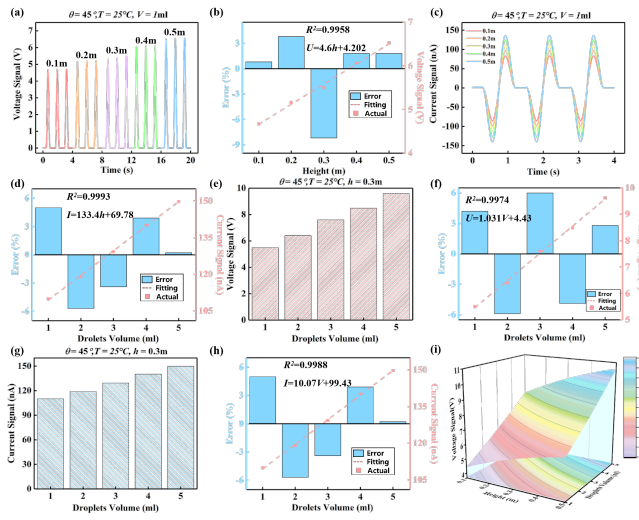
The initial h (vertical distance between the burette outlet and the sensor) is 0.3 m , and deionized water (DI water) droplets with 1 mL are firstly used to characterize the sensor's performance. According to the previous studies [21]–[23],

[30], the incident angle between the droplets and the sensor has a significant impact on the detection performance of the sensor. As shown in Fig. 2(b), when the Θ increases from 15° to 75° , the output current signal increases initially and reaches the maximum of 110 nA at 45° before progressively decreasing from 45° to 75° . This is because while the Θ is lower than 45° , the leakage can not slip off quickly after the contacts as the nearly horizontal sensor surface, which leaves a layer on the surface and shields the electrostatic induction effect. On the other hand, the effective contact area between the droplets and sensor is insufficient, leading to a small output performance. Generally, the optimal incident angle of the TLLS is 45° , while the response signal for different angles demonstrates the potential in identify leakage direction information.

Since high-temperature elements in power and cabin equipments, the cabin temperature can reach 45°C , the leakage droplets may carry high temperature, which is considered to be a key factor affecting the dielectric constant and polarity of the droplets [45]. Under the condition of $\Theta = 45^\circ$, as the T increase from 25°C to 45°C , the output voltage and current signals decrease from 5.5V to 1.3V and 110nA to 61nA respectively, which is shown in Fig. 2(c) and Fig. 2(d). The experimental results can be explained by the relationship among the dielectric constant, polarity, and the T [44], [45]:

$$-10^6 \frac{\partial^2 \ln d}{\partial^2 \ln P} = 2a_1 + 4a_2 T + 4a_3 p + 8a_4 p T \quad (1)$$

In this equation, T represents temperature, P stands for pressure, d signifies the dielectric constant of water, while constant a_1 , a_2 , a_3 , a_4 , p are associated with operational temperature. The increase in temperature leads to an increase in conductivity, and a decrease in dielectric constant and triboelectric charge density, resulting in a decrease in the output performance of the TLLS. The above experimental results show that the TLLS is capable of detecting leakage droplets temperature and substances which change the dielectric and polar properties. Furthermore, the pH value of the liquid in the ship's pipeline is weakly acidic or alkaline, such as lubricating oil, sewage, and seawater. Therefore, the effect of the leakage droplets with different pH value on the TLLS performance is also investigated. As shown in Fig. 2(e) and Fig. 2(f), under the condition of $\Theta = 45^\circ$, $T = 25^\circ\text{C}$, $V = 1\text{ mL}$, $h = 0.3\text{ m}$, as the pH various from 5 to 9, the output voltage and current signal are almost constant, meaning that the application of



(a) Response voltage performance under $\Theta = 45^\circ$, $V = 1 \text{ mL}$, $T = 25^\circ\text{C}$, $pH = 7$, h from 0.1 m to 0.5 m . (b) LOOCV validation for evaluating accuracy and generalization performance of the h and output voltage signal. (c) Response current performance due to $\Theta = 45^\circ$, $V = 1 \text{ mL}$, $T = 25^\circ\text{C}$, $pH = 7$, h from 0.1 to 0.5 m . (d) LOOCV validation for evaluating accuracy and generalization performance of the h and output current. (e) The output voltage performance of TLLS under $\Theta = 45^\circ$, $h = 0.3 \text{ m}$, $T = 25^\circ\text{C}$, $pH = 7$, V from 1 ml to 5 ml . (f) LOOCV validation for evaluating accuracy and generalization performance of the $V-U$ model. (g) The output current performance of TLLS with $\Theta = 45^\circ$, $h = 0.3 \text{ m}$, $T = 25^\circ\text{C}$, $pH = 7$, V from 1 ml to 5 ml . (h) LOOCV validation for evaluating accuracy and generalization performance of the $V-I$ model. (i) Relationship between the output voltage signal of the TLLS, the height, and the droplet volume.

the TLLS is less affected by pH and further expanding the application area.

Under the condition of the $V = 1 \text{ ml}$, $\Theta = 45^\circ$, $T = 25^\circ\text{C}$, $pH = 7$, the influence of the h on the output performance of the TLLS is demonstrated in Fig. 3(a) and Fig. 3(c). As the h increase from 0.1 m to 0.5 m , the output voltage and current signal increase from 4.7 V to 7.4 V and 83 nA to 136 nA respectively, which could be explained by the following formulas [46]:

$$V = \frac{h\sigma}{\varepsilon_0} \quad (2)$$

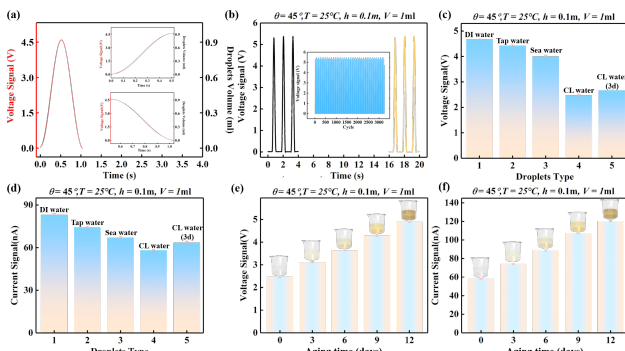
Where h is the distance between the droplets and the coating, ε_0 is the the vacuum permittivity, σ is the triboelectric charge density.

$$Q = -\left(\frac{Q_0 d_1}{h \varepsilon_w + d_1}\right) \quad (3)$$

Where Q_0 is the charges of the droplets, d_1 is the thickness of SiO_2/PTFE coating , and ε_w is the relative permittivity of the coating. Since ε_0 , σ , Q_0 , d_1 , and ε_w are relative constant during the contact process, the increase h leads to an increment of the sensor output signal. Furthermore, Fig.

3(b) and Fig. 3(d) indicates the relationship between h and output performance of the sensor via Leave One out Cross-Validation (LOOCV) strategy, with correlation coefficients of 0.9958 and 0.9993 . The main causes of errors are equipment vibration and noise interference in the environment. It is worth noting that the capacity of the TLLS detecting the leakage height information shows great potential in online and real time ship pipeline leakage location. Fig. 3(e) and Fig. 3(g) shows the effect of the V on the sensor output performance. As the V increase from 1 ml to 5 ml , with the condition of $\Theta = 45^\circ$, $h = 0.3 \text{ m}$, $T = 25^\circ\text{C}$, $pH = 7$, the output voltage and current signal increase from 5.5 V to 9.61 V and 83 nA to 141.5 nA , respectively, as shown in Fig. 3(f) and Fig. 3(h). Also, the linearity among the V and output performance reaches 0.9974 and 0.9988 , demonstrating that as the h and V of the droplets increases, the kinetic energy of the droplets increases in the dripping process, resulting in an increase in the output performance. Fig. 3(i) demonstrates the relationship among the output voltage signal, the height, and the droplet volume. The response surface reflects the interaction between the two factors and the influence of each factor on the output voltage signal, and meanwhile the shape of the equal-height line reflects the strength of the effect of the two factors. It is obvious that the droplet volume has a bigger influence on the output voltage signal of the TLLS, which is caused by as the volume increases, the contact area between the droplet and the TLLS increases gradually yet the small amount of droplets splashes as height increase. Through experimental data investigation and analysis, TLLS has a high accuracy and robustness in detecting the height and volume information of the droplet, especially for the low liquid level volumes or minor droplets, indicating that the TLLS can be effectively applied to the assessment of the leakage conditions.

As shown in Fig. 4(a), the response time of the TLLS is less than 20 ms , highlighting that the unique ability of the sensors to acquire the real-time state of droplets and measure the parameters of the moving droplets with greater accuracy. The durability trial of the TLLS is shown in Fig. 4(b), the sensor maintains a steady electrical signal output after repeated impacts by an external load over 3000 cycles. Furthermore, due to the diversity of the liquid types transported in the ship pipeline, the effect of the droplets type on the output signal of TLLS is also investigated. Fig. 4(c) and Fig. 4(d) shows the sensor output performance response to the different K

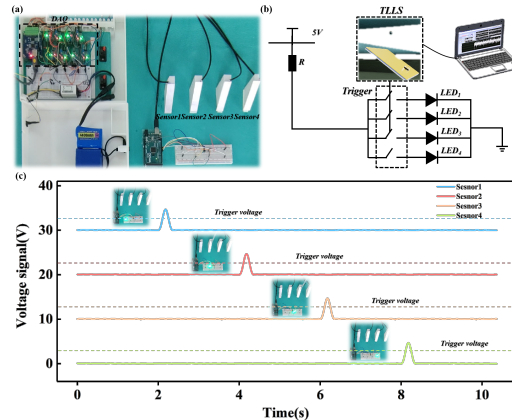


(a) Response time of the TLLS. (b) The durability of the TLLS tested for 3300 cycles. (c) Response voltage signals due to $\Theta = 45^\circ$, $T = 25^\circ\text{C}$, $V = 1 \text{ ml}$, $h = 0.1 \text{ m}$, and different K . (d) Response current signals due to $\Theta = 45^\circ$, $T = 25^\circ\text{C}$, $V = 1 \text{ ml}$, $h = 0.1 \text{ m}$, and different K . (e) Response voltage signals due to $\Theta = 45^\circ$, $T = 25^\circ\text{C}$, $V = 1 \text{ ml}$, $h = 0.1 \text{ m}$, and different aging time of the CL water. (f) Response current signals due to $\Theta = 45^\circ$, $T = 25^\circ\text{C}$, $V = 1 \text{ ml}$, $h = 0.1 \text{ m}$, and different aging time of the CL water.

under the condition of $V = 1 \text{ ml}$, $h = 0.1 \text{ m}$, $\Theta = 45^\circ$, $T = 25^\circ\text{C}$. Obviously, the sensor's output caused by deionized water droplets is the maximum, while the output caused by cooling water(CL water) droplets is the minimum. This phenomenon is caused by the initial charge carried by each droplet and the difference in the induced triboelectric charges during the liquid-solid interaction process, taking seawater as an example, high ion concentration of the droplet may interrupt the contact charging between the droplets and the TLLS [47]. Interestingly, the output caused by the 3 day aging cooling water is much higher than the unused cooling water, which is significant components of the ship cooling system. To further investigate the effect of the aging time on the TLLS output performance, 0d, 3d, 6d, 9d, and 12d aging CL water are employed. As shown in the Fig. 4(e) and Fig. 4(f), as the increase of aging time, the TLLS output performance gradually increases and reaches a peak at 15.18 V, 143 nA regarding 12d aging time. This is because the increase of the aging time increases the metal impurities inside the cooling water, which enhances the electrostatic induction between the droplets and the sensor. The experimental results confirm that the capacity of the TLLS in leakage droplet types identification and the potential in cooling water condition evaluating.

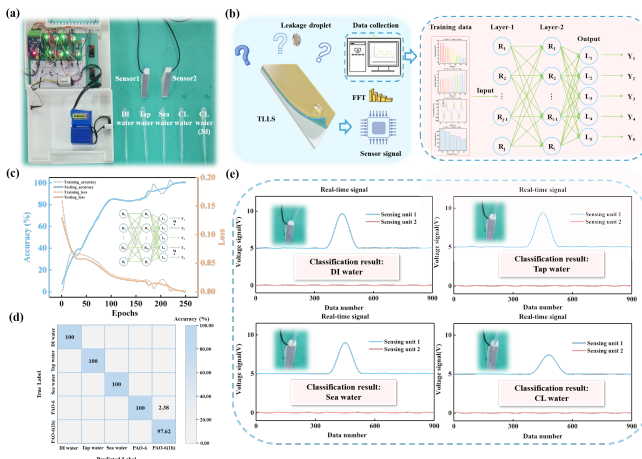
C. Application demonstration of TLLS in real-time leakage detection and location

Figure. 5(a) indicates the photography of the experimental electronic setup, which is comprised of four TLLSs, a data



(a) Response time of the TLLS. (b) The durability of the TLLS tested for 3300 cycles. (c) Response voltage signals due to $\Theta = 45^\circ$, $T = 25^\circ\text{C}$, $V = 1 \text{ ml}$, $h = 0.1 \text{ m}$, and different K . (d) Response current signals due to $\Theta = 45^\circ$, $T = 25^\circ\text{C}$, $V = 1 \text{ ml}$, $h = 0.1 \text{ m}$, and different K . (e) Response voltage signals due to $\Theta = 45^\circ$, $T = 25^\circ\text{C}$, $V = 1 \text{ ml}$, $h = 0.1 \text{ m}$, and different aging time of the CL water. (f) Response current signals due to $\Theta = 45^\circ$, $T = 25^\circ\text{C}$, $V = 1 \text{ ml}$, $h = 0.1 \text{ m}$, and different aging time of the CL water.

acquisition (DAQ) module, a control board, and four LEDs. The data acquisition (DAQ) system is composed of four amplifiers and an AD7606 for signal acquisition and data processing, with a data acquisition frequency of 500 Hz. The sensors output a 0-10 V signal, which exceeds the ADC's -5 V to +5 V input range. To address this, the amplifiers apply a 0.5 dB scaling factor to the sensor output, bringing the voltage within the required input range of the ADC. During the data processing, the event detection via determining if the peak voltage signal of the TLLS satisfies the setting value as 3V after the system initialization. When the peak voltage signal meets the setting value, the control board (Arduino Due R3 Mega 2560) is used to control the on/off status of the LED. This framework provides TLLS with the capability to convert the sensory signals of small liquid leaks into the control of LED switches for issuing warnings. The schematic electric circuit connection is depicted in Figure. 5(b). If the voltage signal generated by the contact and separation process between the liquid leakage and the TLLS satisfies the setting values, the electric circuit drives the corresponding LED to turn on. Figure. 5(c) demonstrates how the TLLS is used to control the condition of LEDs by a setting value (see Supplementary Movie S1), since the stability and robustness, the output voltage signals are much larger than the noise signal. The application of TLLS in real-time liquid leakage detection and location reveals that the TLLS has great potential



(a) The photography of the experimental setup. (b) Schematic of signal acquisition and training process. (c) Accuracy and loss results of training and test sets. (d) Confusion map of the training result. (e) The classification results of the proposed intelligent system.

in effectively leakage information capturing and directional leakage warning.

D. Application demonstration of TLLS in liquid leakage classification

Contrary to traditional analysis methods that focus on obtaining shadow features like frequencies and peak numbers, machine learning, as a recent emerging technique for capturing nuances, has been utilized for data collection and pattern analysis of triboelectric signals, offering access to the integration of artificial intelligence (AI) technology with triboelectric sensor to develop a novel intelligent system [34]. Furthermore, this method has the capacity to resolve delicate information for complex characteristics in higher dimensions that are not visible to the naked eye after training the model. Artificial neural network (ANN) is one of the machine learning techniques that are massively successful at solving classification issues with high accuracy and scalability, and it has wildly developed in environmental factors analysis, and parameter recognition (or more detail). The TLLS combined with a lightweight ANN-based predicting model is thus a novel and effective solution for ship pipeline liquid leakage detection and classification.

Herein, a lightweight neural network (ANN) model with fast Fourier transform (FFT) is used to feature extraction and model fitting to achieve the liquid leakage type detection and identification for ship pipelines. To construct the FC-ANN model, five liquids consisting of DI water, tap water, sea water, CL water, and CL water (3d) are tested with TLLS under the

same experimental conditions ($V = 1 \text{ ml}$, $h = 0.1 \text{ m}$, $\Theta = 45^\circ$, $T = 25^\circ \text{C}$).

The photography of the experimental setup is shown in Figure. 6(a), the intelligent sensing system consists of two TLLSs, a data acquisition (DAQ) module for data capture and processing, and a visualization user interface based on Matlab software. Noticeably, the voltage signals are recorded for 120 times (one liquid droplet each time), and 300 points length signals are displayed in a visualize window to guarantee the accuracy of the recorded data. These row signals are utilized as features of the samples, which contains incident angle, temperature, height, volume, and type information of the liquid leakage. Figure. 6(b) demonstrates the process of signal acquisition and training, the collected 120 samples are split at the ratio of 4:1:1 (80 samples for training, 20 samples for testing, 20 samples for validation). Under the evaluation of the cross-entropy loss function, the ANN with two fully connected layers (FCLs) has the smallest loss function and the accuracy of the training samples reaches 100% after 250 epochs, which is shown in Figure. 6(c). Meanwhile, as presented in Figure. 6(d), the confusion matrix is utilized to evaluate the positive predictive value and true positive of the two-FCLs ANN, and the classification accuracy reaches 99.5%.

As shown in Fig.S13, the row signals detected by TLLS are processed by FFT in the MCU, and the raw signals undergo a FFT to convert the time-domain signals into the frequency domain. After that, the FFT results are fed into two-FCLs ANN. Meanwhile, the visualization user interface is used to display the real time collected data and the prediction results obtained by the two-FCLs ANN. As shown in Figure. 6(e) and Fig.S12, five liquid types are utilized to test the practical classification accuracy of the intelligent system, and the results demonstrate that the system successfully distinguishes the type of liquid and displays the type information and corresponding voltage signal in the visualization user interface (see Supplementary Movie S2). Thus, the investigation of TLLS arrays based intelligent sensing system presents great promise in practical ship pipelines monitoring and provides a novel method for modern ship pipelines management.

III. CONCLUSION

We propose a triboelectric liquid leakage sensor based on liquid-solid triboelectric nanogenerator for ship pipeline monitoring. The sensor has a superhydrophobic coating that is self-cleaning, wear-resistant, lightweight, cost-effective, and

highly accurate. The coating can be integrated with existing steel structures to form large-scale sensor networks without disassembling the pipelines. With the unique superhydrophobic coating components, the TLLS effectively enhances adaptability and eliminates the deficiency of low reliability in the harsh cabin environment. On the basis of the induction law and analysis model, an intelligent sensing system composed of TLLS arrays and a lightweight artificial neural network is proposed, which reveals the robustness and accuracy in leakage droplets detection, location, and classification. The sensing system offers a creative method for modern ship pipeline monitoring and has great potential for unmanned ship applications. Moreover, the sensing system can evaluate the condition of cooling water in real-time and online which is crucial for ship cooling system performance. Our work opens up new possibilities for oil condition monitoring and triboelectric sensor design.

IV. METHODS

Fabrication of TLLS

The fabrication process of the proposal triboelectric sensor is as follows: Firstly, 1 ml KH-560 and 15 ml deionized water are mixed in a beaker under ambient conditions and acetic acid is used to change the pH value to 5, the solution is then stirred for 10 minutes at 40°C. Next, 10 ml acidic SiO₂ sols are added to the solution and reacted for two hours under ambient conditions. After the reaction, the modified Si sols are obtained. Then, 10 ml PTFE emulsions and 2.5 ml DMF are added to the modified Si sols under ambient conditions and acetic acid is used to change the pH value to 5. After that, the solution is well stirred for 20 minutes under ambient conditions to form the suspension. Finally, the suspension is uniformly sprayed by the spray gun on the surface of the GH901 steel sheet (50 mm in length, 20 mm in widths, 2.5 mm in thickness) and dried at 250 °C for 3 h. The thickness of SiO₂-PTFE coating is 0.3-0.5 mm, which is measured by thickness gauge.

COMPETING INTERESTS

The authors declare no Competing Financial or Non-Financial Interests.

DATA AVAILABILITY

The datasets generated during and/or analysed during the current study are available from the corresponding author on

reasonable request.

REFERENCES

- [1] W. Zhang, P. Wang, K. Sun, C. Wang, and D. Diao, "Intelligently detecting and identifying liquids leakage combining triboelectric nanogenerator based self-powered sensor with machine learning," *Nano Energy*, vol. 56, pp. 277–285, 2019.
- [2] H. H. Yin, H. Chen, and Z. B. Peng, "Real-time model method research in ship pipeline system leakage detecting," in *Applied Mechanics and Materials*, vol. 105. Trans Tech Publ, 2012, pp. 685–688.
- [3] K. B. Adedeji, Y. Hamam, B. T. Abe, and A. M. Abu-Mahfouz, "Towards achieving a reliable leakage detection and localization algorithm for application in water piping networks: An overview," *IEEE Access*, vol. 5, pp. 20272–20285, 2017.
- [4] Y. Zhang, J. Wu, S. Zhang, and P. Su, "Design of ship pipeline diagnostic control system based on mass flow," in *2019 IEEE 4th Advanced Information Technology, Electronic and Automation Control Conference (IAEAC)*, vol. 1. IEEE, 2019, pp. 1718–1721.
- [5] T. R. Sheltami, A. Bala, and E. M. Shakshuki, "Wireless sensor networks for leak detection in pipelines: a survey," *Journal of Ambient Intelligence and Humanized Computing*, vol. 7, no. 3, pp. 347–356, 2016.
- [6] M. A. Adegbeye, W.-K. Fung, and A. Karnik, "Recent advances in pipeline monitoring and oil leakage detection technologies: Principles and approaches," *Sensors*, vol. 19, no. 11, p. 2548, 2019.
- [7] O. Scussel, M. Brennan, F. C. Almeida, J. Muggleton, E. Rustighi, and P. Joseph, "Estimating the spectrum of leak noise in buried plastic water distribution pipes using acoustic or vibration measurements remote from the leak," *Mechanical Systems and Signal Processing*, vol. 147, p. 107059, 2021.
- [8] A. Makeenkov, I. Lapitskiy, A. Somov, and A. Baranov, "Flammable gases and vapors of flammable liquids: Monitoring with infrared sensor node," *Sensors and Actuators B: Chemical*, vol. 209, pp. 1102–1107, 2015.
- [9] R.-q. Lv, H.-k. Zheng, Y. Zhao, and Y.-f. Gu, "An optical fiber sensor for simultaneous measurement of flow rate and temperature in the pipeline," *Optical Fiber Technology*, vol. 45, pp. 313–318, 2018.
- [10] S. C. Bera, "A low-cost centrifugal force type flow sensor for measuring the flow rate of a fluid through a pipeline," *IEEE Sensors Journal*, vol. 7, no. 8, pp. 1206–1210, 2007.
- [11] C. A. Diaz, A. Leal-Junior, C. Marques, A. Frizera, M. J. Pontes, P. F. Antunes, P. S. Andre, and M. R. Ribeiro, "Optical fiber sensing for sub-millimeter liquid-level monitoring: A review," *IEEE Sensors Journal*, vol. 19, no. 17, pp. 7179–7191, 2019.
- [12] S. Ali, S. B. Qaisar, H. Saeed, M. Farhan Khan, M. Naeem, and A. Anpalagan, "Network challenges for cyber physical systems with tiny wireless devices: A case study on reliable pipeline condition monitoring," *Sensors*, vol. 15, no. 4, pp. 7172–7205, 2015.
- [13] J. Krautkrämer and H. Krautkrämer, *Ultrasonic testing of materials*. Springer Science & Business Media, 2013.
- [14] W. M. Alabaidi, E. A. Alkuam, H. M. Al-Rizzo, E. Sandgren *et al.*, "Applications of ultrasonic techniques in oil and gas pipeline industries: A review," *American Journal of Operations Research*, vol. 5, no. 04, p. 274, 2015.
- [15] S. Datta and S. Sarkar, "A review on different pipeline fault detection methods," *Journal of Loss Prevention in the Process Industries*, vol. 41, pp. 97–106, 2016.

- [16] Y. Yu, A. Safari, X. Niu, B. Drinkwater, and K. V. Horoshenkov, "Acoustic and ultrasonic techniques for defect detection and condition monitoring in water and sewerage pipes: A review," *Applied Acoustics*, vol. 183, p. 108282, 2021.
- [17] L. Long, W. Liu, Z. Wang, W. He, G. Li, Q. Tang, H. Guo, X. Pu, Y. Liu, and C. Hu, "High performance floating self-excited sliding triboelectric nanogenerator for micro mechanical energy harvesting," *Nature communications*, vol. 12, no. 1, pp. 1–10, 2021.
- [18] M. Xu, T. Zhao, C. Wang, S. L. Zhang, Z. Li, X. Pan, and Z. L. Wang, "High power density tower-like triboelectric nanogenerator for harvesting arbitrary directional water wave energy," *ACS nano*, vol. 13, no. 2, pp. 1932–1939, 2019.
- [19] H. Wang, Z. Fan, T. Zhao, J. Dong, S. Wang, Y. Wang, X. Xiao, C. Liu, X. Pan, Y. Zhao *et al.*, "Sandwich-like triboelectric nanogenerators integrated self-powered buoy for navigation safety," *Nano Energy*, vol. 84, p. 105920, 2021.
- [20] J. Luo, W. Gao, and Z. L. Wang, "The triboelectric nanogenerator as an innovative technology toward intelligent sports," *Advanced Materials*, vol. 33, no. 17, p. 2004178, 2021.
- [21] X. Wang, P. Xu, Z. Ma, S. Wang, G. Xie, and M. Xu, "A bio-inspired whisker sensor based on triboelectric nanogenerators," in *2020 35th Youth Academic Annual Conference of Chinese Association of Automation (YAC)*. IEEE, 2020, pp. 105–109.
- [22] X. Wang, P. Xu, J. Liu, S. Wang, T. Chen, T. Guan, J. Tao, and M. Xu, "Semi-flexible bionic whisker sensor based on triboelectric nanogenerators," in *2021 International Conference on Artificial Intelligence and Electromechanical Automation (AIEA)*. IEEE, 2021, pp. 194–198.
- [23] X. Wang, J. Liu, S. Wang, J. Zheng, T. Guan, X. Liu, T. Wang, T. Chen, H. Wang, G. Xie *et al.*, "A self-powered triboelectric coral-like sensor integrated buoy for irregular and ultra-low frequency ocean wave monitoring," *Advanced Materials Technologies*, p. 2101098.
- [24] M. Xu, S. Wang, S. L. Zhang, W. Ding, P. T. Kien, C. Wang, Z. Li, X. Pan, and Z. L. Wang, "A highly-sensitive wave sensor based on liquid-solid interfacing triboelectric nanogenerator for smart marine equipment," *Nano Energy*, vol. 57, pp. 574–580, 2019.
- [25] C. Zhang, L. Liu, L. Zhou, X. Yin, X. Wei, Y. Hu, Y. Liu, S. Chen, J. Wang, and Z. L. Wang, "Self-powered sensor for quantifying ocean surface water waves based on triboelectric nanogenerator," *Acs Nano*, vol. 14, no. 6, pp. 7092–7100, 2020.
- [26] S. Wang, P. Xu, X. Wang, J. Zheng, X. Liu, J. Liu, T. Chen, H. Wang, G. Xie, J. Tao *et al.*, "Underwater bionic whisker sensor based on triboelectric nanogenerator for passive vortex perception," *Nano Energy*, vol. 97, p. 107210, 2022.
- [27] H. Yang, J. Hu, H. Yang, W. Liu, Z. Wang, Q. Zeng, Q. Li, D. Zhang, Y. Xi, and Z. L. Wang, "A multifunctional triboelectric nanogenerator based on conveyor belt structure for high-precision vortex detection," *Advanced Materials Technologies*, vol. 5, no. 10, p. 2000377, 2020.
- [28] Y. Wang, J. Wang, X. Xiao, S. Wang, P. T. Kien, J. Dong, J. Mi, X. Pan, H. Wang, and M. Xu, "Multi-functional wind barrier based on triboelectric nanogenerator for power generation, self-powered wind speed sensing and highly efficient windshield," *Nano Energy*, vol. 73, p. 104736, 2020.
- [29] Y. Wang, C. Wu, and S. Yang, "A self-powered rotating speed sensor for downhole motor based on triboelectric nanogenerator," *IEEE Sensors Journal*, vol. 21, no. 4, pp. 4310–4316, 2020.
- [30] P. Xu, X. Wang, S. Wang, T. Chen, J. Liu, J. Zheng, W. Li, M. Xu, J. Tao, and G. Xie, "A triboelectric-based artificial whisker for reactive obstacle avoidance and local mapping," *Research*, vol. 2021, 2021.
- [31] P. Wang, L. Pan, J. Wang, M. Xu, G. Dai, H. Zou, K. Dong, and Z. L. Wang, "An ultra-low-friction triboelectric–electromagnetic hybrid nanogenerator for rotation energy harvesting and self-powered wind speed sensor," *ACS nano*, vol. 12, no. 9, pp. 9433–9440, 2018.
- [32] S.-J. Park, S. Lee, M.-L. Seol, S.-B. Jeon, H. Bae, D. Kim, G.-H. Cho, and Y.-K. Choi, "Self-sustainable wind speed sensor system with omnidirectional wind based triboelectric generator," *Nano Energy*, vol. 55, pp. 115–122, 2019.
- [33] W. Zhong, L. Xu, F. Zhan, H. Wang, F. Wang, and Z. L. Wang, "Dripping channel based liquid triboelectric nanogenerators for energy harvesting and sensing," *Acs Nano*, vol. 14, no. 8, pp. 10 510–10 517, 2020.
- [34] Q. Zhou, J. Pan, S. Deng, F. Xia, and T. Kim, "Triboelectric nanogenerator-based sensor systems for chemical or biological detection," *Advanced Materials*, vol. 33, no. 35, p. 2008276, 2021.
- [35] Q.-T. Nguyen and K.-K. K. Ahn, "Fluid-based triboelectric nanogenerators: A review of current status and applications," *International Journal of Precision Engineering and Manufacturing-Green Technology*, vol. 8, no. 3, pp. 1043–1060, 2021.
- [36] Y. Feng, L. Zhang, Y. Zheng, D. Wang, F. Zhou, and W. Liu, "Leaves based triboelectric nanogenerator (teng) and teng tree for wind energy harvesting," *Nano Energy*, vol. 55, pp. 260–268, 2019.
- [37] R. Wen, J. Guo, A. Yu, J. Zhai, and Z. I. Wang, "Humidity-resistive triboelectric nanogenerator fabricated using metal organic framework composite," *Advanced Functional Materials*, vol. 29, no. 20, p. 1807655, 2019.
- [38] K. Y. Lee, J. Chun, J.-H. Lee, K. N. Kim, N.-R. Kang, J.-Y. Kim, M. H. Kim, K.-S. Shin, M. K. Gupta, J. M. Baik *et al.*, "Hydrophobic sponge structure-based triboelectric nanogenerator," *Advanced materials*, vol. 26, no. 29, pp. 5037–5042, 2014.
- [39] R. Cramer, R. Tulalian, P. Angelo, M. Van Stuijvenberg, and D. Shaw, "Detecting and correcting pipeline leaks before they become a big problem," in *SPE Middle East Oil & Gas Show and Conference*. OnePetro, 2015.
- [40] B. Wang, Y. Wu, Y. Liu, Y. Zheng, Y. Liu, C. Xu, X. Kong, Y. Feng, X. Zhang, and D. Wang, "New hydrophobic organic coating based triboelectric nanogenerator for efficient and stable hydropower harvesting," *ACS applied materials & interfaces*, vol. 12, no. 28, pp. 31 351–31 359, 2020.
- [41] W. Xu, X. Zhou, C. Hao, H. Zheng, Y. Liu, X. Yan, Z. Yang, M. Leung, X. C. Zeng, R. X. Xu *et al.*, "Slips-teng: robust triboelectric nanogenerator with optical and charge transparency using a slippery interface," *National science review*, vol. 6, no. 3, pp. 540–550, 2019.
- [42] R. N. Wenzel, "Surface roughness and contact angle," *The Journal of Physical Chemistry*, vol. 53, no. 9, pp. 1466–1467, 1949.
- [43] G. Akerlof and H. Oshry, "The dielectric constant of water at high temperatures and in equilibrium with its vapor," *Journal of the American Chemical Society*, vol. 72, no. 7, pp. 2844–2847, 1950.
- [44] Q. Liang, X. Yan, X. Liao, and Y. Zhang, "Integrated multi-unit transparent triboelectric nanogenerator harvesting rain power for driving electronics," *Nano Energy*, vol. 25, pp. 18–25, 2016.
- [45] G. Akerlof and H. Oshry, "The dielectric constant of water at high temperatures and in equilibrium with its vapor," *Journal of the American Chemical Society*, vol. 72, no. 7, pp. 2844–2847, 1950.
- [46] Q. Liang, Z. Zhang, X. Yan, Y. Gu, Y. Zhao, G. Zhang, S. Lu, Q. Liao, and Y. Zhang, "Functional triboelectric generator as self-powered vibration sensor with contact mode and non-contact mode," *Nano Energy*, vol. 14, pp. 209–216, 2015.
- [47] L. Xie, L. Yin, Y. Liu, H. Liu, B. Lu, C. Zhao, T. A. Khattab, Z. Wen, and X. Sun, "Interface engineering for efficient raindrop solar cell," *ACS nano*, vol. 16, no. 4, pp. 5292–5302, 2022.



First A. Author Xinyu Wang is currently pursuing his doctor's degree in Nankai University and University of Lille, China. His current research interests include smart textiles, self-powered sensing system and control, and triboelectric nanogenerators.



Fifth E. Author, Jr. Jinshan Yang is currently pursuing his doctor's degree in Nankai University, China. His current research interests include modeling and control of flexible spacecraft, deep reinforcement learning, embedded control systems and their applications.



Second B. Author Xiaodong Jiao is currently pursuing the Ph.D. degree in control science and engineering with the College of Artificial Intelligence, Nankai University, Tianjin. His research interests include Modeling and analysis of chaotic system, acoustic manipulation.



Sixth F. Author, Jr. Tangzhen Guan is currently pursuing the bachelor's degree in Dalian Maritime University, China. His current research interests in the self-powered system and triboelectric nanogenerators.



Third C. Author, Jr. Pengyu Liang is currently pursuing his master's degree in Nankai University, China. His current research interests include aircraft control and target recognition in the field of computer vision.



Seventh G. Author, Jr. Hao Sun received the Ph.D. degree in control science and engineering from the College of Artificial Intelligence, Nankai University, Tianjin, in 2019. He is currently a Research Assistant with Nankai University. His current research interests include intelligent control, evolutionary optimization, dynamic modeling, and their application in parafoil systems.



Forth D. Author, Jr. Fei Zelin, an engineer at the Beijing Institute of Spacecraft Environment Engineering, is currently pursuing a master's degree at Tsinghua University, specializes in the field of spacecraft thermal environmental simulation.



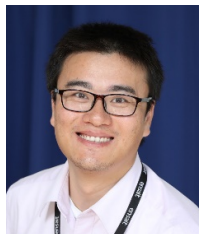
Eighth H. Author, Jr. Jin Tao received the Ph.D. degree in control science and engineering from Nankai University, Tianjin, China, in 2017. His research interests include intelligent control, evolutionary optimization, and multi-agent systems.



Forth D. Author, Jr. Wenxuan Guo is currently pursuing his master's degree in Nankai University, China. His current research interests in the self-powered sensing system and triboelectric nanogenerators.



Xianyi Zeng is a chair professor in ENSAIT –University of Lille, France, Director of the GEMTEX National Laboratory, and also a guest professor of Soochow University, Nankai University and Xi' An Polytechnic University. He is an IEEE Senior Member, President of the Textile, Bioengineering and Informatics Society, and President of the Group on Human-Machine Systems of GRAISyHM.



and virtual textile.

Tenth J. Author, Jr. Xuyuan Tao received the Ph.D. degree in automation from the Lille University of Science and Technology, Villeneuve d' Ascq, France, in 2010. Since 2011, he has been an Associate Professor with the ENSAIT Textile Engineering Institute, Roubaix, France. His research interests include multifunctional and intelligent textiles, flexible sensors and actuators,



Fourteenth N. Author, Jr. Qinglin Sun received the M.S. degree from Tianjin University, Tianjin, China, in 1990, and the Ph.D. degree in control theory and control engineering from Nankai University, Tianjin, China, in 2003. In 1998, he joined the College of Artificial Intelligence, Nankai University, Tianjin, China, where he is a Full Professor. His research interests are adaptive control, active disturbance rejection control, flexible aircraft modeling and control.



operation and maintenance technology.

Eleventh K. Author, Jr. Xingjia Jiang has been with Dalian Maritime University where he is currently an associate professor since 2011. He received his B.S. and M.S. from Dalian Maritime University in China in 2007 and 2010. His current research work focuses on energy harvesting and self-powered sensor based on triboelectric nanogenerator and Intelligent ship



Twelfth L. Author, Jr. Peng Xu is currently pursuing his doctor degree in Dalian Maritime University, China. His current research interests include self-powered sensing system and control, bio-inspired design and control for marine and underwater robots and triboelectric nano-generators.



blue energy, self-powered systems, tri-

Thirteenth M. Author, Jr. Minyi Xu received his Ph.D. degree from Peking University in 2012. During 2016 –2017, he joined Professor Zhong Lin Wang' group at Georgia Institute of Technology. Now he is a Professor in the Marine Engineering College, Dalian Maritime University. His current research is mainly focused on the areas of blue energy, self-powered systems, tri-

boelectric nanogenerators and its practical applications in smart ship and ocean.